772 *Biochemistry* **2010,** *49,* 772–781
DOI: 10.1021/bi9013006

BIOCHEMISTRY
including biophysical chemistry & molecular biology
Article

Estrogen Receptor Interactions and Dynamics Monitored in Live Cells by Fluorescence Cross-Correlation Spectroscopy[†]

Julien Savatier,[‡,§] Stéphan Jalaguier,[§] Matthew L. Ferguson,[‡] Vincent Cavaillès,[§] and Catherine A. Royer*[,‡]

[‡]*Centre de Biochimie Structurale, INSERM U554, and CNRS UMR5048, Université Montpellier 1 and 2, Montpellier F-34090, France and* [§]*IRCM, Institut de Recherche en Cancérologie de Montpellier, INSERM, U896, Université Montpellier 1, and CRLC Val d'Aurelle Paul Lamarque, Montpellier F-34298, France*

Received July 28, 2009; Revised Manuscript Received December 26, 2009

ABSTRACT: Quantitative characterization of protein interactions in live cells remains one of the most important challenges in modern biology. In the present work we have used two-photon, two-color, fluorescence cross-correlation spectroscopy (FCCS) in transiently transfected COS-7 cells to measure the concentrations and interactions of estrogen receptor (ER) subtypes α and β with one of their transcriptional coactivator proteins, TIF2, as well as heterodimerization between the two ER subtypes. Using this approach in a systematic fashion, we observed a strong ligand-dependent modulation of receptor−coactivator complexation, as well as strong protein concentration dependence for complex formation in the absence of ligand. These quantitative values for protein and complex concentrations provide the first estimates for the ER-TIF2 K_d for the full-length proteins and in a cellular context (agonist, $<\sim$6 nM; antagonist, $>\sim$3 μM; unliganded, ~200 nM). Coexpression of the two ER subtypes revealed substantial receptor heterodimer formation. They also provide, for the first time, estimated homo- and heterodimerization constants found to be similar and in the low nanomolar range. These results underscore the importance of receptor and coregulator expression levels and stability in the tissue-dependent modulation of receptor function under normal and pathological conditions.

The human estrogen receptors (ERs)[1] are transcriptional activators, belonging to the homodimeric steroid hormone receptor subfamily of nuclear receptors. This subfamily, which also includes the androgen, progesterone, glucocorticoid, and mineralocorticoid receptors, controls the expression of a large number of mammalian genes responsible for sexual development and reproduction, as well as metabolism, growth, and differentiation. The human ERs are expressed from two different highly homologous genes to yield the α and β subtypes. These two ERs have markedly different tissue distributions, exhibit ligand specificity, and play opposite roles in the regulation of cell proliferation (*1*). They both act primarily via interactions with specific estrogen response elements present in the promoter regions of target genes, and for certain promoters, the ER heterodimer is thought to be required for activation (*2*−*4*). Depending on the presence and identity of small hormone ligands, the ERs will recruit either transcriptional coactivators or corepressors that perform chromatin remodeling functions and interact with other downstream transcription factors to modulate gene expression and ultimately the physiological state of the organism. The first identified and well-characterized coactivators belong to the so-called p160 family which consists of three related members, SRC1, SRC2 (also called TIF2 or NCoA2), and SRC3 (*5*). These coregulators contain two separate transcription activation domains and function primarily by recruiting histone-modifying enzymes. The deregulation of ER function is involved in a number of human pathologies, including breast and ovarian cancers. Given their central role in human health and disease, it is not surprising that ERs have been the target of intensive study, both from a fundamental perspective and as the target of multiple drug development programs. Consequently, a great deal is known concerning the molecular mechanisms of ER function and the structural basis for ligand-dependent modulation of ER transcriptional activity (reviewed in ref *6*). Moreover, the physiopathology of ER-based diseases and the effects of various ligands have been well documented (*7*−*10*). Despite such intensive efforts at the molecular and physiological levels, a more complete understanding of ER function and its modulation under particular physiopathological circumstances will require the quantitative biophysical information about ER interactions and dynamics in physiologically relevant environments that to date have only been accessible *in vitro* (*11*−*14*).

In recent years, novel fluorescence microscopy techniques have advanced the frontiers of quantitative measurements in live cells, tissues, organs, and even whole multicellular organisms. Among these approaches, fluorescence fluctuation and correlation spectroscopy is especially appealing for situations in which one wishes to measure the degree of interaction between two protein partners (*15*−*23*). Pioneered for *in vitro* applications, this approach has been used in several instances to measure biomolecular interactions in live cells (*24*−*42*). As explained in the review by Bacia and Schwille (*43*), this approach involves simultaneous

[†]The work was made possible by an instrumentation grant from the Association pour la Recherche contre le Cancer to CAR and a research grant from the Agence National pour la Recherche (ReCoFLuo) to C.A.R. and V.C. M.L.F. was the recipient of an International Research Postdoctoral Fellowship (OISE 0710816) from the National Science Foundation.

*Corresponding author. Tel: +33 467 41 79 02. Fax: +33 467 41 79 13. E-mail: catherine.royer@cbs.cns.fr.

[1]Abbreviations: ER, estrogen receptor; FCS, fluorescence correlation spectroscopy; FCCS, fluorescence cross-correlation spectroscopy; Tif2, P160 coactivator also called SRC2 or NCoA2; mCherry, fluorescent protein monomeric cherry; cer, fluorescent protein cerulean; FP, fluorescent protein; E2, agonist 17β-estradiol; ICI, antagonist ICI182780; NLS, nuclear localization signal; ERE, estrogen response element; RLU, relative light units; PBS, phosphate-buffered saline; APD, avalanche photodiode; CCD, charge-coupled device.

 Published on Web 12/29/2009

excitation, using a variety of strategies (*44*−*46*), among them a femtosecond pulsed IR laser for simultaneous two-photon excitation (*47*) of two biomolecules bearing two fluorescent dyes. The time correlation of their intensity in two different detection channels, along with the autocorrelation of their individual fluorescence in single channels, allows calculation of the total concentration of each species, free and bound, and hence the degree of complex formation between two proteins. These measurements can also allow for the determination of complex stoichiometries (*40*, *48*). Despite the recent progress made in the application of FCCS to live cell studies, the relatively small number of reports in the literature (~20) attests to the fact that such studies still represent a considerable technical challenge and remain far from routine. Nonetheless, the possibility to measure directly in live cells total protein concentration and protein−protein complex formation promises to open large avenues of research in signal transduction and more generally in the protein interaction field. In particular, beyond proof of principle, new insights into the functional role of protein interactions require systematic studies under a variety of physiological conditions.

In the present work, we have used two-photon, two-color fluorescence cross-correlation spectroscopy to measure the interactions of ERα and ERβ with one of their transcriptional coregulator proteins, TIF2 (*49*). The ER proteins were studied as N-terminal fusions of the blue fluorescent protein (FP), cerulean (*50*), whereas the coregulator was fused to mCherry (*51*). This FP pair was chosen to avoid cross-talk which leads to artifacts in the cross-correlation. We also investigated ER subtype heterodimerization by transfecting cerulean and mCherry fusions of ERα and ERβ. The results allowed us to estimate, for the first time, the affinities between these protein complexes for the full-length proteins. Moreover, these values are determined in a live cell environment. Altogether, these data suggest that protein expression levels are key in regulating ER function in certain cell and tissue types and provide information concerning the dynamic behavior and spatial localization of the free proteins and complexes, thus defining the conditions under which complexation occurs and the degree of heterogeneity among the cell population.

MATERIALS AND METHODS

Fluorescent Protein Constructs. pmCerulean-C1 was a gift from D. Piston (Vanderbilt University, Nashville, TN). pmCherry-C1 was constructed as follows: The insert encoding mCherry (a gift from R. Tsien, University of California San Diego) was PCR amplified taking pRSETB-Cherry as a template and then ligated into pmCerulean-C1 previously digested with *Nhe*I and *Bsp*EI. mCherry was PCR amplified using pRSETB-Cherry as a template and then ligated into pEYFP-TIF2 (a gift from V. Georget, Institut de Biologie Intégrative, CNRS, Paris, France) previously digested with *Nhe*I and *Bgl*II to create pmCherry-TIF2. The cDNA encoding human ERα was excised from pEGFP-ERα (donated by P. Balaguer, IRCM, Montpellier, France) with *Xho*I and *Bam*HI and then inserted into pmCerulean-C1 and pmCherry-C1 previously digested with the same restriction enzymes to create respectively pmCerulean-ERα and pmCherry-ERα. The cDNA encoding hERβ was excised from pNGV1-ERβ (donated by S. Mosselman, Organon, Oss, The Netherlands) by *Bam*HI and then inserted into pmCerulean-C1 previously digested with the same enzyme to create pmCerulean-ERβ. pmCerulean-NLS and pmCherry-NLS were constructed as follows: The cDNA encoding the nuclear localization signal (NLS) of SV40 T antigen was ligated into respectively pmCerulean-C1 and pmCherry-C1 previously digested with *Eco*RI and *Bam*HI. NLS-cerulean was PCR amplified using pmCerulean-C1 as a template and then inserted into pmCherry-C1 to create pmCherry-NLS-cerulean. The ERE-βGlob-Luc reporter construct has been described elsewhere (*52*, *53*).

Cell Culture and Transfection. COS-7 cells were maintained in Dulbecco's modified Eagle's:F12 medium (DMEM:F12) supplemented with 10% fetal calf serum (Invitrogen, Carlsbad, CA) and an antibiotic solution (Invitrogen). For reporter assay experiments, cells were deprived of steroids for 5 days in phenol red free medium supplemented with 3% dextran-coated charcoal-stripped serum (DCC-DMEM:F12), plated in 24-well dishes (10^5 cells/well), and transfected using Jet-PEI (Ozyme, Saint-Quentin-en-Yvelines, France). In all experiments, the amount of transfected DNA was kept constant using the pcDNA3 plasmid (1 μg of total DNA), and pCMV-β-gal (200 ng) was used to normalize the transfection efficiency. Twenty hours after transfection, and 24 h before lysis, medium was replaced by DCC-DMEM:F12 supplemented with 10^{-8} M 17β-estradiol (E2 from Sigma-Aldrich, St. Louis, MO) and ICI182780 (ICI from Astrazeneca, Rueil-Malmaison, France). Cells were then harvested in a lysis buffer (25 mM Tris−H_3PO_4 (pH 7, 8), 2 mM DTT, 2 mM EDTA, 1% Triton X-100, and 10% glycerol), and the luciferase activity was measured by the reaction of lysate with the luciferin solution (270 μM coenzyme A, 470 μM luciferin, 530 μM ATP, 20 mM Tris−H_3PO_4, 1.05 mM $MgCl_2$, 2.7 mM $MgSO_4$, 0.1 mM EDTA, and 33 mM DTT). Luciferase activity was measured as relative light units (RLU) on a luminometer. All values represent the mean RLU/β-galactosidase (±SD) from triplicates.

For imaging, cells were deprived of steroids for 5 days in phenol red free medium supplemented with 3% dextran-coated charcoal-stripped serum (DCC-DMEM:F12), plated in Lab-Tek chambered coverglass two-well dishes (Nunc Thermo Fisher Scientific, Roskilde, Denmark) at 3×10^5 cells/well, and transfected after 1 day using JetPEI or FuGene6 (Invitrogen). After 24 h and at least 2 h before imaging medium was replaced two times by PBS and then by DCC-DMEM:F12 supplemented with 10^{-8} M E2 or ICI or with the same volume of pure ethanol (1.5 μL) as control condition. pH was stabilized by 10 mM HEPES buffer (Gibco, Paislay, Scotland). Cells were then kept at 37 °C before imaging.

Imaging Conditions. For the majority of the experiments, three two-well dishes were alternatively used and stored at 37 °C in a humidified chamber supplied with 5% CO_2 near the microscope. Each dish was used only 20 min maximum at a time at room temperature in order to avoid low-temperature effects on cells. FCS acquisitions each require about 2 min. After that we improved our setup with a thermoregulated system (Cube 2 + Box; Life Imaging Services, Basel, Switzerland), covering the microscope in order to maintain a stable 37 °C temperature. The heater was turned on the day before the experiment to avoid thermal expansion during acquisition. It allowed us to use the same dish more than 20 min at a time. We note that no difference in behavior was observed between the data collected at room temperature (21 °C) and data obtained at 37 °C. Cells were localized using the halogen lamp and DIC visualization. Then cells for imaging were manually chosen using an X-Cite 120 lamp (Exfo, Mississauga, Canada) as epifluorescence excitation, connected to the slider of the microscope by an optical fiber. A 10%

neutral density filter was used to avoid photobleaching, and a double band filter was used to observe only red and blue fluorescence. We also used a CCD camera (Zeiss, Jena, Germany) under some conditions to be able to detect cells expressing very low levels of FPs. When a cell expressing both FPs at appropriate levels was found, it was imaged at different Z positions with two-photon excitation, as explained below.

Fusion Proteins: Imaging and Activity. The two ERs and their coactivator, TIF2, were expressed in COS-7 cells (which lack endogenous ER) as N-terminal fusions with the blue FP, cerulean (cer-ER) (*50*), and mCherry (mCherry-TIF2) (*51*), respectively, which are predominantly monomeric and display relatively good photophysical properties. More importantly, however, these FPs were chosen to eliminate bleed-through from the blue detection channel into the red channel, since such bleed-through is 100% cross-correlated and hence would introduce a substantial artifact into the FCCS measurements. The images obtained for separate expression of mCherry-TIF2 (Supporting Information Figure 1A) or cer-ER (Supporting Information Figure 1B for cer-ERβ) and data not shown for cer-ERα demonstrated that reasonable detection levels can be achieved exciting at 950 nm, using less than 10 mW at the microscope entrance to limit photobleaching. These images revealed a uniquely nuclear localization for both proteins, as expected. The lack of any signal above the dark counts in the red channel when cer-ER is expressed, and likewise in the blue channel when mCherry-TIF2 is expressed, demonstrated that our choice of FPs indeed eliminated the problem of bleed-through. Moreover, we noted that the lack of any signal above the dark counts of the APD detectors in the cytoplasm of the cells surrounding the nuclei or in the nuclei of the channels of the unexpressed FPs also demonstrated that, at this excitation wavelength, cellular autofluorescence and laser background are negligible, an added benefit of the relatively far-IR two-photon excitation. Photobleaching was limited significantly by keeping the excitation intensity low and using only data sets for which it was not the dominant factor. Moreover, for data sets in which bleaching was observed, the portions of the intensity vs time plots for which photobleaching was strong were deleted, and only those portions for which the intensity was relatively stable were analyzed. Histogram analysis (*17*) of multiple fluctuation data sets (data not shown) with concentrations ranging over 2 orders of magnitude yielded good fits with linked molecular brightness values. Under the same excitation conditions (10 mW at 950 nm) cer-ERα exhibited an average molecular brightness of 3000 cpspm (dimer) and that of cer-ERβ was slightly higher, 4500 cpspm (dimer), whereas the average molecular brightness of mCherry-TIF2 under these conditions was 2600 cpspm (monomer). We found no relationship between the molecular brightness and the degree of complex formation.

The transactivation potential of the fusion proteins was also tested with respect to the nonfusion proteins using luciferase assays (Supporting Information Figure 2A−C). On average, the degree of activation of cer-ERα or cer-ERβ by 17β-estradiol (E2, the natural agonist) was nearly equivalent to that of the ERα or ERβ. The reduction in activation upon incubation with the full antagonist, ICI182780, was, for both cer-ERα and cer-ERβ, equivalent to that observed for the nonfluorescent proteins. Finally, the ability of mCherry-TIF2 to activate either ER subtype in the presence of agonist was also found to be equivalent to that of the nonfusion TIF2. The activity of two mutant fusion proteins was also tested (Supporting Information Figure 3A,B). Cer-ERβ bearing a double mutation (L490A/L491A) in the ligand-dependent activation function 22 (AF2) domain (*54*) was, as expected, not capable of transcriptional activation upon agonist binding. Furthermore, a cer-ERα variant bearing a mutation in the DNA binding domain (DBD) that abolishes specific recognition of estrogen response element (ERE) sites (*55*) also did not activate transcription in our ERE-based luciferase assay.

Fluorescence Cross-Correlation Spectroscopy. FCCS measurements were conducted using a setup based on a dual channel ISS Alba fluorescence correlation detector (ISS, Champaign, IL) with avalanche photodiodes and a Zeiss Axiovert 200 microscope (Zeiss, Jena, Germany). The sample was excited by means of a Mai Tai HP fs IR tunable laser (Spectra-Physics, Newport, Mountain View, CA) tuned to 935 or 950 nm. The two-photon cross section of cerulean (*50*) and mCherry has been reported (*56*). The excitation light was focused into the sample by a Zeiss Apochromat 63X oil immersion objective (numerical aperture 1.4), and an E700 SP 2P dichroic filter (Chroma Technology Corp., Rockingham, VT) was used to eliminate the contribution of the IR excitation light in the detected signal. In the FCCS experiments performed a 505 nm dichroic mirror was used to split the detected light onto two channels, and additional 653 ± 50 and 455 ± 50 nm band-pass filters were set before channels 1 and 2, respectively (Chroma Technology Corp., Rockingham, VT). The excitation power was set at <10 mW at the scope entrance in all FCCS measurements. This power was determined to be a threshold one at which the autocorrelation traces became excitation power independent, in order to avoid excitation saturation effects (*57*, *58*) as well as photobleaching (*59*). The microscope was equipped with a Piezo-electric stage (Madcity, Madison, WI) for 3D imaging.

Data Analysis. Focusing a femtosecond pulsed infrared excitation laser beam through a high numerical aperture objective into a sample containing fluorescent species generates a tiny open volume element defined by two-photon excitation probability. In an FCCS experiment, molecules labeled with two spectrally different dyes are simultaneously excited, and the fluctuations in the fluorescence emission in this small volume are detected in two separate channels. In these experiments, three curves are generated by time correlation of the fluorescence intensity fluctuations detected, two autocorrelation functions arising from the blue and red fluorophores $G_B(\tau)$ and $G_R(\tau)$ and one cross-correlation function, which accounts for the molecules in which the two fluorophores diffuse together, $G_x(\tau)$. The autocorrelation and cross-correlation functions can be written as follows, in the absence of cross-talk:

$$G_i(\tau) = \frac{\langle \delta F(t)\delta F(t+\tau)\rangle}{\langle F(t)\rangle^2} \quad (1)$$

$$G_x(\tau) = \frac{\langle \delta F_B(t)\delta F_R(t+\tau)\rangle}{\langle F_B(t)\rangle\langle F_R(t)\rangle} \quad (2)$$

where τ is the lag time. In the particular case of a system of freely diffusing species and assuming a 3D Gaussian excitation profile, closed expressions are derived from eq 1 and eq 2:

$$G_i(\tau) = G_i(0)(1+\tau/\tau_{Di})^{-1}(1+\omega_0^2\tau/z_0^2\tau_{Di})^{-1/2} \quad (3)$$

$$G_x(\tau) = G_x(0)(1+\tau/\tau_{Dx})^{-1}(1+\omega_0^2\tau/z_0^2\tau_{Dx})^{-1/2} \quad (4)$$

where i = B or R (blue or red). ω_0 and z_0 are the waist and length, respectively, of the three-dimensional Gaussian excitation volume at which the intensity drops to $1/e^2$. Here, τ_{Di} and τ_{Dx} are the translational diffusion times of species i and of the complex, respectively, and $G_i(0)$ and $G_x(0)$ are the amplitudes of the auto- and cross-correlation functions, respectively.

If no changes in the brightness of the fluorophores occur upon complexation, the amplitudes of the auto- and cross-correlation curves can be expressed as follows:

$$G_i(0) = \frac{1}{V_{\text{eff}} C_{i,\text{t}}} \tag{5}$$

$$G_x(0) = \frac{C_x}{V_{\text{eff}} C_{\text{G,t}} C_{\text{R,t}}} \tag{6}$$

where i = B or R, $V_{\text{eff,TPE}} = (\pi/2)^{3/2}\omega_0^2 z_0$, and $C_{i,\text{t}}$ and C_x are the total concentration of species i and of the complex, respectively.

In general, the amplitudes of the auto- and cross-correlation curves for similarly diffusing species of different brightness can be expressed as

$$G_{\text{B}}(0) = \sum_i \eta_{i,\text{B}}^2 C_i / V_{\text{eff}} \left(\sum_i \eta_{i,\text{B}} C_i \right)^2 \tag{7}$$

$$G_{\text{R}}(0) = \sum_i \eta_{i,\text{R}}^2 C_i / V_{\text{eff}} \left(\sum_i \eta_{i,\text{R}} C_i \right)^2 \tag{8}$$

$$G_x(0) = \sum_i \eta_{i,\text{B}} \eta_{i,\text{R}} C_i / V_{\text{eff}} \left(\sum_i \eta_{i,\text{B}} C_i \right) \left(\sum_i \eta_{i,\text{R}} C_i \right) \tag{9}$$

In the case of Cer-ERα and mCherry-ERβ, which could form stable homodimers and heterodimers, it was necessary to take the brightness into account in the determination of concentrations from the correlation function amplitudes. We assumed three diffusing species. The Cer-ERα-mCherry-ERβ heterodimer has concentration $C_{\alpha\beta}$ and brightness $\eta_{\text{B},\alpha\beta}$ and $\eta_{\text{R},\alpha\beta}$. The Cer-ERα homodimer has concentration $C_{2\alpha}$ and brightness $\eta_{\text{B},2\alpha}$. The mCherry-ERβ homodimer has concentration $C_{2\beta}$ and brightness $\eta_{\text{R},2\beta}$. Since total concentrations measured were above the expected nanomolar binding affinity for both hetero- and homodimers, Cer-ERα and mCherry-ERβ monomers were not taken into account. We took the brightness of the homodimer to be twice that of the heterodimer for each detector. With this assumption the equations reduce to

$$G_{\text{B}}(0) = \frac{C_{\alpha\beta} + 4C_{2\alpha}}{V_{\text{eff}}(C_{\alpha\beta} + 2C_{2\alpha})^2} \tag{10}$$

$$G_{\text{R}}(0) = \frac{C_{\alpha\beta} + 4C_{2\beta}}{V_{\text{eff}}(C_{\alpha\beta} + 2C_{2\beta})^2} \tag{11}$$

$$G_x(0) = \frac{C_{\alpha\beta}}{V_{\text{eff}}(C_{\alpha\beta} + 2C_{2\alpha})(C_{\alpha\beta} + 2C_{2\beta})} \tag{12}$$

We then solved eqs 10−12 using the function SOLVE in Maxima Version 5.18.1 to determine the concentrations of each species.

The dissociation constant for Cer-ERα and mCherry-TIF2 in the absence of ligand was estimated by comparison of the experimentally determined fractional complex formation with respect to total ERα at the experimentally determined ER and TIF2 concentrations for 40 cells with the results of simulations of the fractional of complex with respect to total ERα as a function of the concentration of TIF2 at five different concentrations of ERα and at interaction free energies ranging from −10 to −7 kcal/mol every 0.5 kcal/mol. Simulations were performed using the BIOEQS software (*60*) as previously described (*61*). The K_{d} was taken to be that corresponding to the simulation for which the most data points fell within the concentrations of the simulations. Heterodimer and homodimer dissociation constants were also estimated based on simulations using the same BIOEQS software. Full global analysis was not feasible since the system involved three dissociation constants and five species in a random concentration titration (we do not control the concentrations of the proteins expressed).

RESULTS

ER-TIF2 Complex Formation. To measure ER-TIF2 interactions, fluorescence correlation measurements and imaging were carried out for transiently transfected COS-7 cells coexpressing cer-ERα or cer-ERβ with the coactivator, mCherry-TIF2, in the absence of any ligand, in the presence of the natural agonist E2, or in the presence of the full antagonist, ICI. For cer-ERα, over 440 FCS acquisitions on over 120 cells and for cer-ERβ over 280 acquisitions on over 60 cells were obtained. Shown in Figure 1 (upper panels, ERα; lower panels, ERβ) are example correlation functions (autocorrelation of the red (1) and blue (2) channels and the cross-correlation between the two) obtained from these cells under different ligand conditions, i.e., ethanol only, agonist, or antagonist. High amplitudes of the cross-correlation functions relative to the autocorrelation amplitudes at short delay time (τ) are indicative of a high degree of interaction. Cross-correlation amplitudes in the presence of agonist were on average quite high. We found highly variable, but on average relatively high, cross-correlation amplitudes in the absence of ligand, as well. In contrast, the cross-correlation amplitude observed in the presence of the full antagonist, ICI, was always fairly low, regardless of the amplitude of the auto-correlation functions. For about half of the cells that were imaged and for which fluctuation data were measured, we found no auto- or cross-correlation. Given the high intensity of the fluorescence of such cells, we concluded that the correlation functions tended to zero amplitude due to the high concentration of the proteins transiently expressed. The range over which we were able to measure correlation was between 6 nM and 3 μM.

As a control, we carried out FCS/FCCS experiments using a cer-NLS-mCherry construct, which localizes to the nucleus like the proteins of interest. FCS/FCCS measurements on this construct yielded maximal cross-correlation signals at short τ, as expected for a unimolecular construct bearing the two FPs (Figure 2A). A negative control with mCherry-NLS and cer-NLS was not successful because the nuclear localization was not efficient, and hence very few cells exhibited reasonable fluorescence levels of the two colocalized proteins. However, as an alternative negative control, we observed very low cross-correlation levels (Figure 2B) for the cer-ERβ construct bearing the deleterious double mutation (L490A/L491A) in the AF2 domain which is responsible for coactivator recruitment.

From the Go values of the cross- and autocorrelation functions of the cells coexpressing the receptor and the coactivator, the total

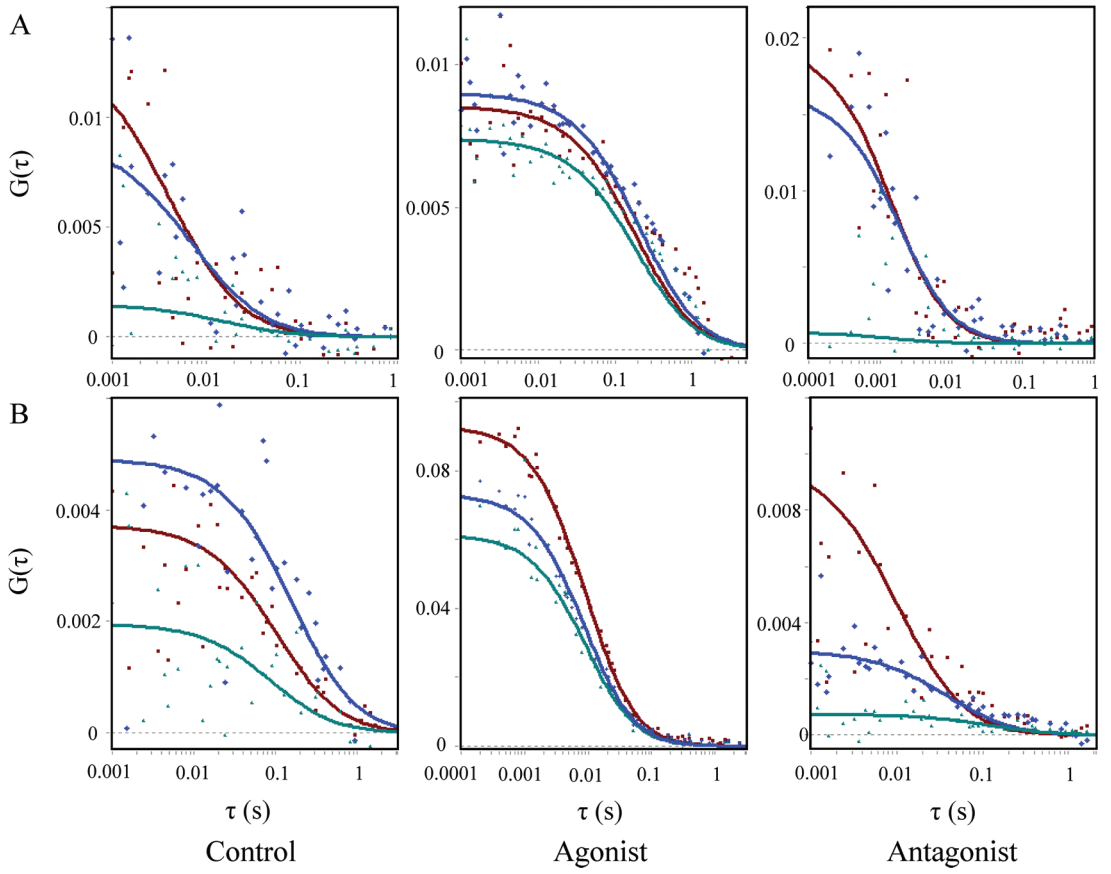

FIGURE 1: ER-TIF2 interactions by FCCS. Examples of correlation curves for different ligand conditions (left panels, control EtOH; middle panels, agonist E2; right panels, antagonist ICI). Each panel represents a unique experiment. (A) cer-ERα + mCherry-TIF2. (B) cer-ERβ + mCherry-TIF2. Curves: red, channel 1 autocorrelation corresponding to mCherry-TIF2; blue, channel 2 autocorrelation corresponding to cer-ERα or cer-ERβ; green, cross-correlation between the two channels.

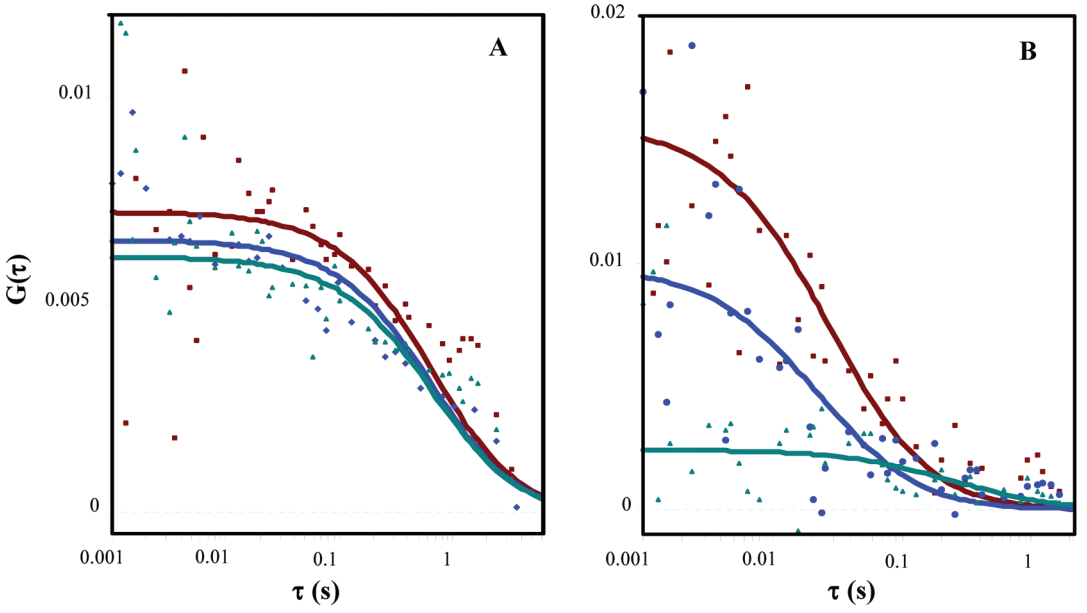

FIGURE 2: Cross-correlation controls. Examples of correlation curves for (A) positive cross-correlation control = mCherry-NLS-cerulean, with EtOH, and (B) negative cross-correlation control = cer-ERβ AF2 mutated + mCherry-TIF2, with agonist E2. Curves: red, channel 1 autocorrelation corresponding to mCherry; blue, channel 2 autocorrelation corresponding to cerulean; green, cross-correlation between the two channels.

concentrations of the cer-ER (α or β) and mCherry-TIF2, as well as that of the ER-TIF2 complexes, were calculated as described in the Materials and Methods section (eqs 5 and 6). The fraction of complex formed was calculated from the ratio of the concentration of the complex with respect to that of the total concentration of the least concentrated of the two proteins (ER or TIF2) in order to reveal the tendency to interact rather than simply the relative concentrations of the two

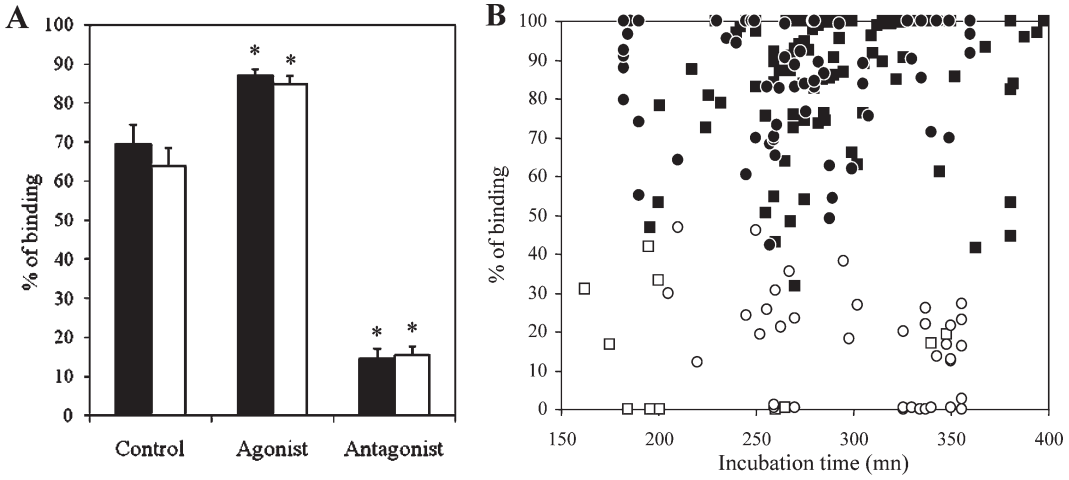

FIGURE 3: Average degree of complex formation. (A) Mean fractional complex formation between cer-ERα (black) or cer-ERβ (white) and mCherry-TIF2 with control (EtOH) and two ligands (agonist, E2; antagonist, ICI) ± SEM (standard error on the mean) (*: values are significantly higher or lower for agonist and antagonist condition, respectively, vs control, $P < 0.001$). (B) Influence of incubation time on fractional complex formation. Fractional complex formation between cer-ERα or cer-ERβ with mCherry-TIF2 at different incubation times with two ligands: agonist, E2; antagonist, ICI. Cer-ERα/mCherry-TIF2 with E2 (■) or ICI (□); cer-ERβ/mCherry-TIF2 with E2 (●) or ICI (○).

proteins. The average fractional complex formation for the control conditions (no ligand) for both receptor subtypes was found to be relatively high and that in the presence of agonist even higher, while the average fractional complex formation in the presence of antagonist was quite low (Figure 3A). The ensemble of all of the values obtained in individual cells for the fractional complex formation from the FCCS measurements on the two ER subtypes in the presence of agonist and antagonist is plotted as a function of time of incubation with the ligand (Figure 3B). We note that there was no effect of incubation time at times longer than the 150 min shown in the figure. Moreover, despite the rather high degree of variability for these values, a clear frontier is evident around 40% complex formation, above which only three antagonist measurements can be observed and below which only one agonist value is found. This underscores the fact that there is a highly significant difference between the degree of complex formation observed in the presence of agonist compared to that observed in the presence of antagonist. These quantitative FCCS measurements directly confirm in individual live cells and in real time ER-coregulator interactions as the molecular basis for the ligand-induced biological response.

These single cell quantitative measurements yield extremely important information beyond these average values of the degree of complex formation. It is important to underline that, for each cell, our FCCS measurements yield the total absolute concentration of each of the proteins, as well. In the case of the ligand-bound receptors, we observed no relationship between the degree of complex formation and the protein concentration (data not shown). For the agonist-bound receptor, for which the average degree of complex formation was quite high, this indicates that the K_d for the interaction must be below the low concentration limit of our experiments (< ~10 nM). Observation in individual cells of intermediate degrees of complex formation in the presence of agonist arise in part due to the signal-to-noise ratio in our measurements but may reflect as well the effects of cell cycle on these regulatory interactions. In the case of antagonist-bound receptors, the degree of complex formation remained low (well below 50%), even at the highest protein concentrations observed, indicating that the K_d for the interaction is higher than these values (> ~2 μM).

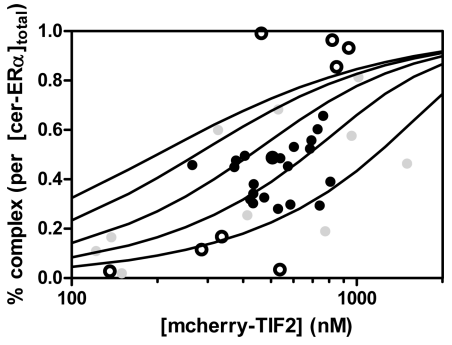

FIGURE 4: Degree of complex formation in the absence of ligand. Fractional cer-ERα-mCherry-TIF2 complex formation with respect to the total ERα concentration for measurements taken for a number of cells in the absence of ligand as a function of both cer-ERα and mCherry-TIF2 concentration. Lines correspond to the fractional complex formation as a function of Tif2 concentration simulated using a K_d of 200 nM for ERα concentrations of 50, 200, 500, 1000, and 2000 nM from left to right. Filled circles correspond to measurements for which the degree of complex formation corresponded to ERα concentrations between the two closest simulation lines. Gray circles are measurements for which the fraction of complex with respect to total ERα high or too low by a factor of less than 10%, with respect to the nearest simulated lines. Finally, the open circles correspond to measurements for which the fraction complex differs by over 10% from the nearest simulated lines.

In the absence of ligand, our FCS/FCCS data revealed a higher average degree of complex formation than did the transactivation assays carried out on the entire cell population. This is because cells chosen for FCCS measurements expressed both proteins at concentrations of over 100 nM, whereas the transactivation assays were carried out for the whole population for which the transfection efficiency is quite heterogeneous. For this reason, bulk measurements on transiently transfected cells tend to underestimate protein interactions. More importantly, using FCS/FCCS we observed a protein concentration dependence of the degree of complex formation in the absence of ligand. This indicated that binding could be occurring under equilibrium conditions and that it may be possible to estimate the affinity. The values from ~40 cells for the fraction of complex with respect to the total concentration of cer-ERα are plotted as a function of

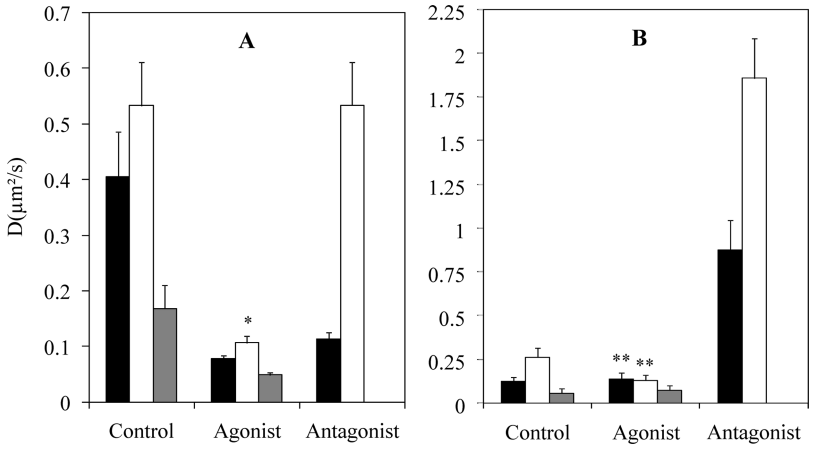

FIGURE 5: Mean diffusion coefficient: (A) coexpressed cer-ERα (black), mCherry-TIF2 (white), and complex (gray) between the two for control and ligand conditions (agonist, E2; antagonist, ICI); (B) coexpressed cer-ERβ (black), mCherry-TIF2 (white), and complex (gray) between the two for control and ligand conditions (agonist, E2; antagonist, ICI). Mean ± SEM (standard error on the mean). Statistical test: values are significantly lower for agonist vs antagonist condition with *, $P < 0.01$, and **, $P < 0.001$. We cannot determine a real diffusion coefficient for the complex in the presence of antagonist since the cross-correlation curve is most of the time close to zero.

the concentration of mCherry-TIF2 in Figure 4. We have also simulated for several values of affinity (ΔG from −10 to −7 kcal/mol every 0.5 kcal/mol) the degree of complex formation (with respect to total ERα) as a function of TIF2 for several total ERα concentrations between 50 nM and 2 μM. The majority of the points (filled circles) fall between ERα concentration lines corresponding to a complex K_d value of 200 nM (lines in Figure 4), while a few (gray circles) exhibit a degree of complex formation within 10% of that consistent with the ER and TIF2 concentrations and predicted by the 200 nM K_d. A few points (open circles) lie far from the expected degree of interaction consistent with their ER concentrations and with this K_d. We conclude therefore that the affinity between ERα and TIF2 in the absence of ligand is near 200 nM.

Diffusion times can also be determined from analysis of the autocorrelation profiles, providing some information about the dynamics of these proteins in the nucleus. The recovered values varied significantly between cells (Figure 5). For both ERα and ERβ, a large fraction of the measured diffusion coefficients for the ER subtypes were found to be very slow, below 0.5 μm^2/s. Only a few measurements yielded significantly faster diffusion. Moreover, we found no significant correlation between the diffusion coefficients and the total concentration of protein. Hence, the relatively slow diffusion times do not appear to arise from concentration-dependent aggregation. Broken down by ligand condition (Figure 5), ER and TIF2 diffusion appeared to be, on average, slower in the presence of agonist and, in the absence of ligand, slower for the cross-correlation function. These situations correspond to conditions under which the degree of complex formation is maximal and may indicate that the ER-TIF2 complexes bind to chromatin or other nuclear partners with a higher probability than the individual proteins.

Receptor Subtype Heterodimerization. As noted in the introduction, certain promoters in certain tissue types are under the specific control of ERα/ERβ heterodimers. Hence the relative concentration of each of these receptor subtypes, as well as the relative affinities between the homo- and heterodimers, constitute additional levels of transcriptional control. In order to obtain estimates for the ER homo- and heterodimer affinities, we coexpressed cer-ERα and mCherry-ERβ in COS-7 cells and measured heterodimerization by FCCS for a number of different

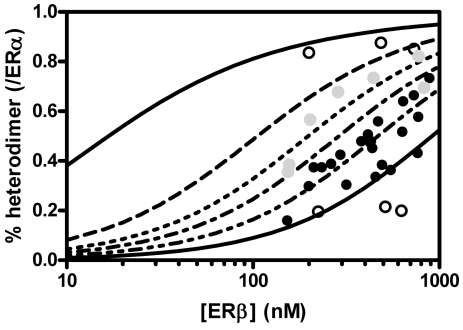

FIGURE 6: Heterodimer formation. Degree of heterodimer formation with respect to the concentration of total ERα (expressed in terms of monomer) as a function of the concentration of mCherry-ERβ (also expressed in terms of monomer). Lines correspond to simulations assuming homo- and heterodimerization constants of 7 and 2.8 nM and 10, 100, 200, 300, 500, and 1000 nM ERα in descending order. Black circles correspond to experimental results for which the ERα concentration falls between the closest corresponding simulation lines. The empty circles correspond to points for which the ERα concentration falls well beyond the corresponding simulation lines. The gray circles correspond to points for which the ERα concentrations are about 2-fold higher than those predicted by the simulations.

cells. The concentrations of the homo- and heterodimers were calculated by solving the set of equations for the Go values of the auto- and cross-correlation functions as described in the Material and Methods section. Although a full global analysis of the data was not feasible, we carried out simulations (described in Materials and Methods) of the degree of heterodimerization expected as a function of ERβ concentration at a series of ERα concentrations, using different values of the free energies for the homo- and heterodimer interactions. The points in Figure 6 correspond to the experimentally determined values of the fractional heterodimer populations (with respect to the total concentration of ERα expressed as monomer) as a function of the concentration of mCherry-ERβ. The lines in Figure 6 correspond to the theoretical values of the fractional heterodimer population for six different concentrations of ERα (10, 100, 200, 300, 500, and 1000 nM) as a function of ERβ concentration, simulated using a heterodimer free energy of interaction of 11.5 kcal/mol (K_d = 2.8 nM) and a homodimer free energy of 11.0 kcal/mol

(K_d = 7 nM) for both ERα and ERβ. The black filled circles correspond to measured values for which the experimental total concentration of ERα falls within the corresponding simulated lines and are hence compatible with the K_d values used for the simulations. The gray circles correspond to ERα concentrations which are within a factor of 2 of those represented by the simulations and hence slightly surpass the expected degree of heterodimerization based on these K_d values. Finally, the six white points correspond to large over- or underestimations of the degree of heterodimerization. The majority of measurements are compatible with the simulated affinities for the homo- and heterodimer in the low nanomolar range. Using K_d values of 16 and 37 nM, we found very poor agreement with the data. Hence, we estimate the uncertainty on these K_d values as less than a factor of 5 (< 1.0 kcal/mol).

DISCUSSION

We have presented here the quantitative measurement of the interaction of the human ER subtypes (α and β) with one of their coactivator partners, TIF2, in live cells using two-photon, two-color FCCS. These results were obtained thanks to a pair of FP proteins that avoids bleed-through and a far-IR excitation wavelength that leads to negligible autofluorescence and minimal bleaching and cellular damage. These are the first such quantitative measurements using the full-length coactivator, as it cannot be overexpressed and purified for *in vitro* measurements. We found a very high degree of interaction in the presence of agonist ligand (> 80%) and relatively high levels of interaction in the absence of ligand as well (> 60%). Given the number of measurements, these values are highly significant. We also observed a highly significant decrease in the degree of protein−protein interactions between both subtypes of human ER with the coactivator, TIF2, upon incubation with the full antagonist, ICI182780 (< 20%) and this in spite of the variations in protein expression levels and complex dynamic behavior inherent in live cell studies. Because these measurements were carried out on single cells using fluctuation techniques, they also provide quantitative measurement of the concentrations of these proteins that can be correlated with their degree of interaction. In the case of the agonist-bound receptor, the protein concentrations were in general well above the K_d. In this case we can provide an upper limit of ~6 nM (near the lower limit of our detection) for the dissociation constant. In the presence of antagonist, the average degree of interaction was quite low, and a lower limit near 3 μM (the upper limit of our detection) can be estimated for the ER-TIF2 K_d in the presence of antagonist. In the case of the unliganded receptor, our detectable concentration range (6 nM to ~3 μM) was within the range of the complex affinity, and we were able to estimate a dissociation constant near 200 nM from global analysis of the fractional complex formation. Indeed, ligand-independent interactions of p160 proteins with ERs have been reported (*62*). These results underscore the fact that ER function in various tissues in the absence of ligands will strongly depend on the expression levels of receptors and coregulators, their posttranslational modification status, and their turnover rates. In addition, modulation of receptor function by partial agonists will also be strongly influenced by protein concentration levels. Typical ER concentrations are thought to be near 20 nM, below the interaction threshold in the absence of ligand. However, overexpression of the receptor, for example in pathological states, or high levels of the coactivators could strongly modulate ER function.

These studies provide, as well, some insight into the dynamic properties of these proteins in the nucleus. A large proportion of the ER molecules diffused extremely slowly, $D \sim 0.5$ μm^2/s, although a proportion of molecules exhibited faster diffusion, above 2−5 μm^2/s. A value of 7 μm^2/s was reported from live cell FCS measurements for freely diffusing PPAR (*36*); hence we conclude that the fraction of ER undergoing relatively fast diffusion that we observe here is likely due to free protein diffusing in the nucleus. The slowly diffusing ER and TIF2 molecules may arise from partial immobilization of the complexes via interactions with chromatin, other protein partners, and/or nuclear structures. A number of groups, using fluorescence recovery after photobleaching (FRAP), have studied ligand-dependent dynamics of nuclear receptors in live cells (*63*−*66*). In the case of ERα, these studies, like ours, reveal that receptor diffusion is apparently more rapid in the absence of ligand and that the coactivator SRC1, like TIF2, a member of the p160 family, exhibits diffusion comparable to that of ERα only in the presence of agonist (*66*, *67*). Tudor and colleagues have observed a similar phenomenon for PPAR diffusion using FCS (*36*).

Finally, for the first time, the affinity of the homo- and heterodimerization of the ER subtypes has been estimated, and we find values in the low nanomolar range that are within experimental error of each other. A low nanomolar K_d for homodimerization is consistent with our *in vitro* ER-DNA binding studies, in which coupling of dimerization to DNA binding is observed in this concentration range (*13*). An estimation of receptor subtype heterodimerization has long been sought after. Unfortunately, luciferase- or β-galactosidase-based transactivation measurements provide no insight whatsoever concerning heterodimer-specific transcriptional activation. Bulk measurements such as BRET (*68*) for heterodimerization provide some idea of heterodimer formation but suffer from false positives, as well as limited sensitivity. In addition, the protein concentration in each cell is not available in such a bulk assay, nor is any information concerning the expression heterogeneity between cells, so no estimations of the affinities can be made.

While the present studies provide convincing quantitative information concerning interaction affinities between these important proteins under different ligation conditions, we are convinced that much further progress can be made. In particular, the variations from cell to cell certainly have multiple sources. First and foremost, the signal-to-noise ratio for the correlation curves must be improved. While the far-IR excitation with a single laser successfully eliminates autofluorescence and provides a perfectly coincident excitation profile for the two fluorophores, the excitation wavelength is clearly not optimal for the molecular brightness, which determines the sensitivity of fluctuation measurements. Improvements are expected from the implementation of scanning FCS, since this will drastically reduce photobleaching and hence allow for an increase in laser power. Some of the observed variations may be of biological origin, and the synchronization of the cells may inform on the importance of this contribution.

In conclusion, we have demonstrated that significant quantitative differences in protein interaction affinities as a function of protein concentration and in response to the binding of small therapeutic ligands of an important class of human steroid hormone receptors implicated in a number of human pathologies can be measured in live cells using two-photon FCCS. Such studies open the perspectives of investigating the effects of

posttranslational modifications, cell cycle, and other environmental factors on the complexes of interest. We note that such phenomena may explain, at least in part, the variability observed for the interactions and the apparent mobility of the proteins studied here. We expect that future investigations using FCCS in live cells will lead to exciting applications in systems biology, signal transduction, and drug screening.

ACKNOWLEDGMENT

The authors thank David Piston of Vanderbilt University and Roger Tsien of the University of California San Diego for the gracious gifts of the plasmids encoding the FPs used in the present study.

SUPPORTING INFORMATION AVAILABLE

Figure 1 demonstrating the lack of channel cross-talk and cellular autofluorescence, Figure 2 giving the results of the luciferase activity assays for the fusion proteins, cer-ERα, cer-ERβ, mCherry-Tif2, with respect to the nonfusion proteins, and Figure 3 giving the results of the luciferase activity assays for the LBD and DBD mutant cer-ERβ proteins with respect to the wild-type cer-ERβ fusion protein. This material is available free of charge via the Internet at http://pubs.acs.org.

REFERENCES

1. Ascenzi, P., Bocedi, A., and Marino, M. (2006) Structure-function relationship of estrogen receptor alpha and beta: impact on human health. *Mol. Aspects Med. 27*, 299–402.
2. Monroe, D. G., Secreto, F. J., Subramaniam, M., Getz, B. J., Khosla, S., and Spelsberg, T. C. (2005) Estrogen receptor alpha and beta heterodimers exert unique effects on estrogen- and tamoxifen-dependent gene expression in human U2OS osteosarcoma cells. *Mol. Endocrinol. 19*, 1555–1568.
3. Pettersson, K., Delaunay, F., and Gustafsson, J. A. (2000) Estrogen receptor beta acts as a dominant regulator of estrogen signaling. *Oncogene 19*, 4970–4978.
4. Tremblay, G. B., Tremblay, A., Labrie, F., and Giguere, V. (1999) Dominant activity of activation function 1 (AF-1) and differential stoichiometric requirements for AF-1 and -2 in the estrogen receptor alpha-beta heterodimeric complex. *Mol. Cell. Biol. 19*, 1919–1927.
5. Xu, J., and Li, Q. (2003) Review of the in vivo functions of the p160 steroid receptor coactivator family. *Mol. Endocrinol. 17*, 1681–1692.
6. Steinmetz, A. C., Renaud, J. P., and Moras, D. (2001) Binding of ligands and activation of transcription by nuclear receptors. *Annu. Rev. Biophys. Biomol. Struct. 30*, 329–359.
7. Howell, A. (2008) The endocrine prevention of breast cancer. *Best. Pract. Res. Clin. Endocrinol. Metab 22*, 615–623.
8. Simpkins, J. W., Yang, S. H., Sarkar, S. N., and Pearce, V. (2008) Estrogen actions on mitochondria—physiological and pathological implications. *Mol. Cell. Endocrinol. 290*, 51–59.
9. Miller, V. M., Jayachandran, M., Hashimoto, K., Heit, J. A., and Owen, W. G. (2008) Estrogen, inflammation, and platelet phenotype. *Gend. Med. 5* (Suppl. A), S91–S102.
10. Maric, C., and Sullivan, S. (2008) Estrogens and the diabetic kidney. *Gend. Med. 5* (Suppl. A), S103–S113.
11. Bourdoncle, A., Labesse, G., Margueron, R., Castet, A., Cavailles, V., and Royer, C. A. (2005) The nuclear receptor coactivator PGC-1-alpha exhibits modes of interaction with the estrogen receptor distinct from those of SRC-1. *J. Mol. Biol. 347*, 921–934.
12. Margeat, E., Bourdoncle, A., Margueron, R., Poujol, N., Cavailles, V., and Royer, C. (2003) Ligands differentially modulate the protein interactions of the human estrogen receptors alpha and beta. *J. Mol. Biol. 326*, 77–92.
13. Margeat, E., Poujol, N., Boulahtouf, A., Chen, Y., Muller, J. D., Gratton, E., Cavailles, V., and Royer, C. A. (2001) The human estrogen receptor alpha dimer binds a single SRC-1 coactivator molecule with an affinity dictated by agonist structure. *J. Mol. Biol. 306*, 433–442.
14. Boyer, M., Poujol, N., Margeat, E., and Royer, C. A. (2000) Quantitative characterization of the interaction between purified human estrogen receptor alpha and DNA using fluorescence anisotropy. *Nucleic Acids Res. 28*, 2494–2502.
15. Williams, R. M., Zipfel, W. R., and Webb, W. W. (2001) Multiphoton microscopy in biological research. *Curr. Opin. Chem. Biol. 5*, 603–608.
16. Denk, W., Strickler, J. H., and Webb, W. W. (1990) Two-photon laser scanning fluorescence microscopy. *Science 248*, 73–76.
17. Chen, Y., Muller, J. D., So, P. T., and Gratton, E. (1999) The photon counting histogram in fluorescence fluctuation spectroscopy. *Biophys. J. 77*, 553–567.
18. Schwille, P., Haupts, U., Maiti, S., and Webb, W. W. (1999) Molecular dynamics in living cells observed by fluorescence correlation spectroscopy with one- and two-photon excitation. *Biophys. J. 77*, 2251–2265.
19. Schwille, P., Korlach, J., and Webb, W. W. (1999) Fluorescence correlation spectroscopy with single-molecule sensitivity on cell and model membranes. *Cytometry 36*, 176–182.
20. Koppel, D. E., Axelrod, D., Schlessinger, J., Elson, E. L., and Webb, W. W. (1976) Dynamics of fluorescence marker concentration as a probe of mobility. *Biophys. J. 16*, 1315–1329.
21. Widengren, J., and Rigler, R. (1998) Fluorescence correlation spectroscopy as a tool to investigate chemical reactions in solutions and on cell surfaces. *Cell. Mol. Biol.* (*Paris*) *44*, 857–879.
22. Rigler, R., Foldes-Papp, Z., Meyer-Almes, F. J., Sammet, C., Volcker, M., and Schnetz, A. (1998) Fluorescence cross-correlation: a new concept for polymerase chain reaction. *J. Biotechnol. 63*, 97–109.
23. Schwille, P., Meyer-Almes, F. J., and Rigler, R. (1997) Dual-color fluorescence cross-correlation spectroscopy for multicomponent diffusional analysis in solution. *Biophys. J. 72*, 1878–1886.
24. Bacia, K., Majoul, I. V., and Schwille, P. (2002) Probing the endocytic pathway in live cells using dual-color fluorescence cross-correlation analysis. *Biophys. J. 83*, 1184–1193.
25. Baudendistel, N., Muller, G., Waldeck, W., Angel, P., and Langowski, J. (2005) Two-hybrid fluorescence cross-correlation spectroscopy detects protein-protein interactions in vivo. *ChemPhysChem 6*, 984–990.
26. Kosturko, L. D., Maggipinto, M. J., Korza, G., Lee, J. W., Carson, J. H., and Barbarese, E. (2006) Heterogeneous nuclear ribonucleoprotein (hnRNP) E1 binds to hnRNP A2 and inhibits translation of A2 response element mRNAs. *Mol. Biol. Cell 17*, 3521–3533.
27. Larson, D. R., Gosse, J. A., Holowka, D. A., Baird, B. A., and Webb, W. W. (2005) Temporally resolved interactions between antigen-stimulated IgE receptors and Lyn kinase on living cells. *J. Cell Biol. 171*, 527–536.
28. Liu, P., Sudhaharan, T., Koh, R. M., Hwang, L. C., Ahmed, S., Maruyama, I. N., and Wohland, T. (2007) Investigation of the dimerization of proteins from the epidermal growth factor receptor family by single wavelength fluorescence cross-correlation spectroscopy. *Biophys. J. 93*, 684–698.
29. Muto, H., Nagao, I., Demura, T., Fukuda, H., Kinjo, M., and Yamamoto, K. T. (2006) Fluorescence cross-correlation analyses of the molecular interaction between an Aux/IAA protein, MSG2/IAA19, and protein-protein interaction domains of auxin response factors of arabidopsis expressed in HeLa cells. *Plant Cell Physiol. 47*, 1095–1101.
30. Ohrt, T., Mutze, J., Staroske, W., Weinmann, L., Hock, J., Crell, K., Meister, G., and Schwille, P. (2008) Fluorescence correlation spectroscopy and fluorescence cross-correlation spectroscopy reveal the cytoplasmic origination of loaded nuclear RISC in vivo in human cells. *Nucleic Acids Res. 36*, 6439–6449.
31. Oyama, R., Takashima, H., Yonezawa, M., Doi, N., Miyamoto-Sato, E., Kinjo, M., and Yanagawa, H. (2006) Protein-protein interaction analysis by C-terminally specific fluorescence labeling and fluorescence cross-correlation spectroscopy. *Nucleic Acids Res. 34*, e102.
32. Rosales, T., Georget, V., Malide, D., Smirnov, A., Xu, J., Combs, C., Knutson, J. R., Nicolas, J. C., and Royer, C. A. (2007) Quantitative detection of the ligand-dependent interaction between the androgen receptor and the co-activator, Tif2, in live cells using two color, two photon fluorescence cross-correlation spectroscopy. *Eur. Biophys. J. 36*, 153–161.
33. Saito, K., Wada, I., Tamura, M., and Kinjo, M. (2004) Direct detection of caspase-3 activation in single live cells by cross-correlation analysis. *Biochem. Biophys. Res. Commun. 324*, 849–854.
34. Slaughter, B. D., Schwartz, J. W., and Li, R. (2007) Mapping dynamic protein interactions in MAP kinase signaling using live-cell fluorescence fluctuation spectroscopy and imaging. *Proc. Natl. Acad. Sci. U.S.A. 104*, 20320–20325.
35. Swift, J. L., Burger, M. C., Massotte, D., Dahms, T. E., and Cramb, D. T. (2007) Two-photon excitation fluorescence cross-correlation

assay for ligand-receptor binding: cell membrane nanopatches containing the human micro-opioid receptor. *Anal. Chem. 79*, 6783–6791.
36. Tudor, C., Feige, J. N., Pingali, H., Lohray, V. B., Wahli, W., Desvergne, B., Engelborghs, Y., and Gelman, L. (2007) Association with coregulators is the major determinant governing peroxisome proliferator-activated receptor mobility in living cells. *J. Biol. Chem. 282*, 4417–4426.
37. Vamosi, G., Baudendistel, N., von der Lieth, C. W., Szaloki, N., Mocsar, G., Muller, G., Brazda, P., Waldeck, W., Damjanovich, S., Langowski, J., and Toth, K. (2008) Conformation of the c-Fos/c-Jun complex in vivo: a combined FRET, FCCS, and MD-modeling study. *Biophys. J. 94*, 2859–2868.
38. Vukojevic, V., Ming, Y., D'Addario, C., Hansen, M., Langel, U., Schulz, R., Johansson, B., Rigler, R., and Terenius, L. (2008) Mu-opioid receptor activation in live cells. *FASEB J. 22*, 3537–3548.
39. Kim, S. A., Heinze, K. G., Waxham, M. N., and Schwille, P. (2004) Intracellular calmodulin availability accessed with two-photon cross-correlation. *Proc. Natl. Acad. Sci. U.S.A. 101*, 105–110.
40. Kim, S. A., Heinze, K. G., Bacia, K., Waxham, M. N., and Schwille, P. (2005) Two-photon cross-correlation analysis of intracellular reactions with variable stoichiometry. *Biophys. J. 88*, 4319–4336.
41. Hink, M. A., Shah, K., Russinova, E., de Vries, S. C., and Visser, A. J. (2008) Fluorescence fluctuation analysis of *Arabidopsis thaliana* somatic embryogenesis receptor-like kinase and brassinosteroid insensitive 1 receptor oligomerization. *Biophys. J. 94*, 1052–1062.
42. Sudhaharan, T., Liu, P., Foo, Y. H., Bu, W., Lim, K. B., Wohland, T., and Ahmed, S. (2009) Determination of in vivo dissociation constant, K_d, of CDC42-effector complexes in live mammalian cells using single wavelength fluorescence cross-correlation spectroscopy (SW-FCCS). *J. Biol. Chem.* (in press).
43. Bacia, K., Kim, S. A., and Schwille, P. (2006) Fluorescence cross-correlation spectroscopy in living cells. *Nat. Methods 3*, 83–89.
44. Kogure, T., Karasawa, S., Araki, T., Saito, K., Kinjo, M., and Miyawaki, A. (2006) A fluorescent variant of a protein from the stony coral Montipora facilitates dual-color single-laser fluorescence cross-correlation spectroscopy. *Nat. Biotechnol. 24*, 577–581.
45. Kogure, T., Kawano, H., Abe, Y., and Miyawaki, A. (2008) Fluorescence imaging using a fluorescent protein with a large Stokes shift. *Methods 45*, 223–226.
46. Thews, E., Gerken, M., Eckert, R., Zapfel, J., Tietz, C., and Wrachtrup, J. (2005) Cross talk free fluorescence cross correlation spectroscopy in live cells. *Biophys. J. 89*, 2069–2076.
47. Heinze, K. G., Koltermann, A., and Schwille, P. (2000) Simultaneous two-photon excitation of distinct labels for dual-color fluorescence crosscorrelation analysis. *Proc. Natl. Acad. Sci. U.S.A. 97*, 10377–10382.
48. Zorrilla, S., Ortega, A., Chaix, D., Alfonso, C., Rivas, G., Aymerich, S., Lillo, M. P., Declerck, N., and Royer, C. A. (2008) Characterization of the control catabolite protein of gluconeogenic genes repressor by fluorescence cross-correlation spectroscopy and other biophysical approaches. *Biophys. J. 95*, 4403–4415.
49. Voegel, J. J., Heine, M. J., Zechel, C., Chambon, P., and Gronemeyer, H. (1996) TIF2, a 160 kDa transcriptional mediator for the ligand-dependent activation function AF-2 of nuclear receptors. *EMBO J. 15*, 3667–3675.
50. Rizzo, M. A., Springer, G. H., Granada, B., and Piston, D. W. (2004) An improved cyan fluorescent protein variant useful for FRET. *Nat. Biotechnol. 22*, 445–449.
51. Shu, X., Shaner, N. C., Yarbrough, C. A., Tsien, R. Y., and Remington, S. J. (2006) Novel chromophores and buried charges control color in mFruits. *Biochemistry 45*, 9639–9647.
52. Castet, A., Boulahtouf, A., Versini, G., Bonnet, S., Augereau, P., Vignon, F., Khochbin, S., Jalaguier, S., and Cavailles, V. (2004) Multiple domains of the receptor-interacting protein 140 contribute to transcription inhibition. *Nucleic Acids Res. 32*, 1957–1966.
53. Balaguer, P., Francois, F., Comunale, F., Fenet, H., Boussioux, A. M., Pons, M., Nicolas, J. C., and Casellas, C. (1999) Reporter cell lines to study the estrogenic effects of xenoestrogens. *Sci. Total Environ. 233*, 47–56.
54. Danielian, P. S., White, R., Lees, J. A., and Parker, M. G. (1992) Identification of a conserved region required for hormone dependent transcriptional activation by steroid hormone receptors. *EMBO J. 11*, 1025–1033.
55. Jakacka, M., Ito, M., Weiss, J., Chien, P. Y., Gehm, B. D., and Jameson, J. L. (2001) Estrogen receptor binding to DNA is not required for its activity through the nonclassical AP1 pathway. *J. Biol. Chem. 276*, 13615–13621.
56. Drobizhev, M., Tillo, S., Markarov, N., Rbane, A., and Hughes, T. E. (2009) Absolute two-photon absorption spectra of orange and red fluorescent proteins. *Biophys. J. 96*, 400a–401a.
57. Nagy, A., Wu, J., and Berland, K. M. (2005) Characterizing observation volumes and the role of excitation saturation in one-photon fluorescence fluctuation spectroscopy. *J. Biomed. Opt. 10*, 44015.
58. Nagy, A., Wu, J., and Berland, K. M. (2005) Observation volumes and {gamma}-factors in two-photon fluorescence fluctuation spectroscopy. *Biophys. J. 89*, 2077–2090.
59. Petrasek, Z., and Schwille, P. (2008) Precise measurement of diffusion coefficients using scanning fluorescence correlation spectroscopy. *Biophys. J. 94*, 1437–1448.
60. Royer, C. A., Smith, W. R., and Beechem, J. M. (1990) Analysis of binding in macromolecular complexes: a generalized numerical approach. *Anal. Biochem. 191*, 287–294.
61. Poujol, N., Margeat, E., Baud, S., and Royer, C. A. (2003) RAR antagonists diminish the level of DNA binding by the RAR/RXR heterodimer. *Biochemistry 42*, 4918–4925.
62. Dutertre, M., and Smith, C. L. (2003) Ligand-independent interactions of p160/steroid receptor coactivators and CREB-binding protein (CBP) with estrogen receptor-alpha: regulation by phosphorylation sites in the A/B region depends on other receptor domains. *Mol. Endocrinol. 17*, 1296–1314.
63. Marcelli, M., Stenoien, D. L., Szafran, A. T., Simeoni, S., Agoulnik, I. U., Weigel, N. L., Moran, T., Mikic, I., Price, J. H., and Mancini, M. A. (2006) Quantifying effects of ligands on androgen receptor nuclear translocation, intranuclear dynamics, and solubility. *J. Cell Biochem. 98*, 770–788.
64. Maruvada, P., Baumann, C. T., Hager, G. L., and Yen, P. M. (2003) Dynamic shuttling and intranuclear mobility of nuclear hormone receptors. *J. Biol. Chem. 278*, 12425–12432.
65. Schaaf, M. J., and Cidlowski, J. A. (2003) Molecular determinants of glucocorticoid receptor mobility in living cells: the importance of ligand affinity. *Mol. Cell. Biol. 23*, 1922–1934.
66. Stenoien, D. L., Patel, K., Mancini, M. G., Dutertre, M., Smith, C. L., O'Malley, B. W., and Mancini, M. A. (2001) FRAP reveals that mobility of oestrogen receptor-alpha is ligand- and proteasome-dependent. *Nat. Cell Biol. 3*, 15–23.
67. Matsuda, K., Nishi, M., Takaya, H., Kaku, N., and Kawata, M. (2008) Intranuclear mobility of estrogen receptor alpha and progesterone receptors in association with nuclear matrix dynamics. *J. Cell Biochem. 103*, 136–148.
68. Powell, E., and Xu, W. (2008) Intermolecular interactions identify ligand-selective activity of estrogen receptor alpha/beta dimers. *Proc. Natl. Acad. Sci. U.S.A. 105*, 19012–19017.